Numerical Analysis of Ca^{2+} Depletion in the Transverse Tubular System of Mammalian Muscle

Oliver Friedrich,* Thomas Ehmer,* Dietmar Uttenweiler,*† Martin Vogel,* Peter H. Barry,‡ and Rainer H. A. Fink*

*Institute of Physiology and Pathophysiology, Medical Biophysics, University of Heidelberg, INF 326, D-69120 Heidelberg, Germany; †Interdisciplinary Center for Scientific Computing, University of Heidelberg, INF 368, D-69120 Heidelberg, Germany; and ‡School of Physiology and Pharmacology, University of New South Wales, Sydney 2052, Australia

ABSTRACT Calcium currents were recorded in contracting and actively shortening mammalian muscle fibers. In order to characterize the influence of extracellular calcium concentration changes in the small unstirred lumina of the transverse tubular system (TTS) on the time course of the slow L-type calcium current (I_{Ca}), we have combined experimental measurements of I_{Ca} with quantitative numerical simulations of Ca^{2+} depletion. I_{Ca} was recorded both in calcium-buffered and unbuffered external solutions using the two-microelectrode voltage clamp technique (2-MVC) on short murine toe muscle fibers. A simulation program based on a distributed TTS model was used to calculate the effect of ion depletion in the TTS. The experimental data obtained in a solution where ion depletion is suppressed by a high amount of a calcium buffering agent were used as input data for the simulation. The simulation output was then compared with experimental data from the same fiber obtained in unbuffered solution. Taking this approach, we could quantitatively show that the calculated Ca^{2+} depletion in the transverse tubular system of contracting mammalian muscle fibers significantly affects the time-dependent decline of Ca^{2+} currents. From our findings, we conclude that ion depletion in the tubular system may be one of the major effects for the I_{Ca} decline measured in isotonic physiological solution under voltage clamp conditions.

INTRODUCTION

One of the main problems in interpreting voltage clamp data in a variety of biological cells including skeletal and heart muscle is the current flow-induced accumulation or depletion of ions due to concentration changes in diffusion restricted near membrane locations, such as in the transverse tubular system (TTS) of skeletal muscle. The TTS consists of a mesh of small tubules as invaginations from the surface membrane and composes ~0.3–0.4% of the fiber volume in frog sartorius muscle (Peachey, 1965) and 0.5–0.6% in rat laryngeal and sternomastoid muscle (Dulhunty, 1982; Hinrichsen and Dulhunty, 1982) and spans throughout the muscle fiber.

According to the Nernst-Planck equation, ion concentration changes such as Ca^{2+} depletion result in reduced driving forces and therefore influence the time course of recorded currents. Ca^{2+} depletion in the TTS has been shown to be a predominant factor in the decay of the slow L-type Ca^{2+} current (I_{Ca}) in frog skeletal muscle fibers using the Vaseline gap technique (Almers et al., 1981). However, under different experimental conditions, Cota et al. (1984) proposed that I_{Ca} decay was due to a voltage-dependent inactivation process in the first place and not due to depletion of tubular Ca^{2+}. With the 3-MVC (three-microelectrode voltage clamp technique) in intact fibers under hypertonic conditions, the decay of I_{Ca} in amphibian skeletal muscle was explained exclusively by a voltage-dependent inactivation mechanism (Cota and Stefani, 1989). However, there is also evidence that tubular Ca^{2+} depletion exists in fibers bathed in isotonic solutions (Almers et al., 1981; Lorkovic and Rüdel, 1983; Friedrich et al., 1999) and in stretched fibers (Cota et al., 1984; Miledi et al., 1983; Nicola-Siri et al., 1980).

Furthermore, previous investigations and simulations of the influence of concentration changes on the calcium currents (I_{Ca}) did not sufficiently include potentially important properties of the calcium channel; for example, the voltage dependence and the intrinsic time course of inactivation (Levis et al., 1983). Thus, the role of Ca^{2+} depletion in the TTS in skeletal muscle is still controversially discussed (Beaty and Stefani, 1976; Stanfield, 1977; Sánchez and Stefani, 1978, 1983; Almers et al., 1981; Almers and Palade, 1981; Cota et al., 1983; Francini and Stefani, 1989; Francini et al., 1992; García et al., 1992).

The aim of this study was to investigate the effect of calcium ion depletion on I_{Ca} in skeletal muscle including the above-mentioned intrinsic channel parameters. We therefore present a method where an experimentally recorded I_{Ca} trace serves as input data for a numerical simulation. The numerical approach was necessary, as the analytical analysis of ion concentration changes and the electrical responses is, in general, not practicable due to the nonlinearity of the underlying processes (Eisenberg et al., 1977; see also Uttenweiler and Fink, 1999). In the first set of our recorded I_{Ca} traces (input data for the simulation) tubular Ca^{2+} ion depletion was impaired by an extracellular buffering agent. From these input data the effect of Ca^{2+} depletion on the

Received for publication 8 March 2000 and in final form 31 January 2001.

Address reprint requests to Prof. Dr. Rainer H. A. Fink, Institute of Physiology and Pathophysiology, Medical Biophysics, Im Neuenheimer Feld 326, D-69120 Heidelberg, Germany. Tel.: +49-(0)-6221-544065; Fax: +49-(0)-6221-544123; E-mail: rainer.fink@urz.uni-heidelberg.de.

0006-3495/01/05/2046/10 $2.00

time course of I_{Ca} in unbuffered solution was calculated. The resulting output was then compared with the experimentally recorded Ca^{2+} currents from the same fiber in unbuffered solution, which did not contain the calcium buffering agent, and thereby allowing Ca^{2+} depletion to occur. Such an approach should also prove most helpful in clarifying the contribution of Ca^{2+} depletion when recording currents in other tissues, e.g., in cardiac and nerve cells (Amsellem et al., 1995; Blatter and Niggli, 1998; Egelman and Montague, 1999).

MATERIALS AND METHODS

Electrophysiology

Muscle preparation and solutions

All experiments were carried out according to the guidelines laid down by the local Animal Care Committee. Interossei muscles from BALB/c mice (2–3 months) were enzymatically isolated (for solutions see below; solution A) and stored in Ringer's solution (B) before the experiments as previously described by Friedrich et al. (1999). Single fibers were then transferred into the recording chamber, which contained the unbuffered recording solution (C). Before the second voltage clamp recording (see below), fibers were perfused up to 20 min with the buffered solution (D) to allow a complete solution exchange in the TTS. The fibers had lengths between 490 μm and 680 μm and diameters in the range of 35–70 μm.

For the solutions, concentrations are given in mM: enzymatic isolation solution (A): 140 NaCl; 4 KCl; 2 $CaCl_2$; 1 $MgCl_2$; 10 HEPES; 1.5 mg/ml collagenase IA (Sigma Chemicals, St. Louis, MO). Ringer's solution (B): 140 NaCl; 4 KCl; 2 $CaCl_2$; 1 $MgCl_2$; 10 HEPES; 11 glucose. Unbuffered isotonic recording solution (C): 10 calcium acetate; 146 TEA-Br; 1 $MgCl_2$; 5 Cs-Br; 5 4-aminopyridine (4-AP); 5 3,4-di-aminopyridine (3,4-DAP); 0.1 KCl; 10 HEPES. Osmolarity was 340 mosmol l^{-1} (Semi-Micro Osmometer Type ML, Knauer, Berlin, Germany). The ionic strength ($\Gamma/2$) was calculated to be 189 mM. Calcium buffered solution (D): 65 $Ca(OH)_2$; ~5 calcium-acetate; 3.2 $Mg(OH)_2$; 60 TEA-Br; 10 HEPES, 115 malic acid (Sigma Chemicals); 5 Cs-Br; 5 4-aminopyridine (4-AP); 5 3,4-di-aminopyridine (3,4-DAP); 0.1 KCl. The osmolarity was nearly the same as in the unbuffered solution.

The pH was adjusted to 7.40 ± 0.02 with NaOH or acetate in all solutions. Voltage-dependent Na^+ channels were blocked by 500 nM TTX in (C) and (D).

Electrical recordings

Two-microelectrode voltage clamp measurements (2-MVC) were carried out as previously described by Friedrich et al. (1999) using a standard voltage clamp device (GeneClamp 500, Axon Instruments, Foster City, CA) with borosilicate pipettes (GB150-F8P) filled with 3 M KCl. Bath temperature was controlled with an accuracy of ±0.1°C via a custom-built analog temperature controlling device based on Peltier elements. Most experiments were carried out at 24°C. In some experiments the temperature was set to 30°C in order to simulate more closely the physiologically relevant temperature for mammalian skeletal muscle. Current and voltage recordings were filtered through an 8-pole Bessel filter and recorded digitally using pClamp6 software (Axon Instruments) on a standard 486 computer. The sampling rate was set to 400 Hz.

In 10 mM Ca^{2+} solution linear currents during a voltage step pulse were subtracted by a leak subtraction box, which subtracts a scaled proportion of the rectangular step pulse from the uncorrected currents recorded (Almers et al., 1981). When blocking the voltage-dependent Ca^{2+} channels with 2 mM verapamil, depolarization to more positive membrane potentials resulted in nonlinear outward currents (Fig. 1 *A*), which could not be compensated for by the linear leak subtraction procedure. Similar outward current components have also been found during the activation of I_{Ca} in mammalian extensor digitorum longus fibers (e.g., by Lamb and Walsh, 1987, see their Fig. 1). As these outward currents displayed a distinct threshold varying from +5 mV to +20 mV in the individual fibers (Fig. 1, *B* and *C*; see also Fig. 4) we restricted the membrane potential to quantitatively analyze calcium currents to depolarizations up to maximally +20 mV.

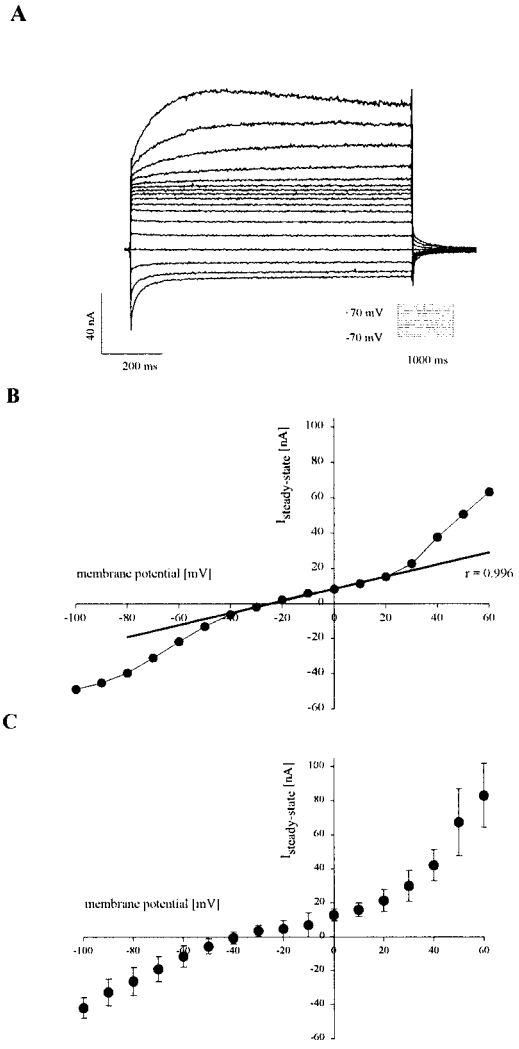

FIGURE 1 Membrane currents in 10 mM Ca^{2+} containing solution with 2 mM verapamil added. (*A*) Membrane currents are shown in the potential range between −100 mV and +60 mV in unbuffered 10 mM Ca^{2+} containing hypertonic solution with 2 mM verapamil added to block L-type Ca^{2+} channels. For potentials more positive than +20 mV a nonlinear outward conductance can be seen. (*B*) The corresponding steady-state *I-V* relation between −40 mV and +20 mV can be considered linear (r = 0.996) for the fiber shown in (*A*), and thus can be removed from the nonlinear currents by the linear leak subtraction method, so that no additional outward component interferes with I_{Ca} in experiments where the L-type channels are not blocked. (*C*) Verifies this *I-V* deviation from the linear behavior for potentials more positive than ~+20 mV in n = 5 fibers.

Thus, under our experimental conditions in almost Cl^--free solution that contained additional Na^+- and K^+-channel blockers (TTX and TEA,

respectively), mainly ion flow through the L-type DHP Ca^{2+} channel contributes to the measured inward current signal and the inward currents shown in the following are almost exclusively slow calcium currents (I_{Ca}). To prevent damage to the fiber due to more vigorous contraction and shortening at higher membrane potentials, pulse durations were reduced by 100 ms for each additional 10-mV step in membrane potential depolarization in experiments covering a wider potential range.

MATHEMATICAL MODELING

For the simulations of the influence of the Ca^{2+} ion concentration changes in the TTS on the time course of I_{Ca}, the experimentally recorded current $I_{exp}^{buf}(t)$ obtained in calcium-buffered solution was used as input data for the numerical simulation. The influence of ion depletion on the time course of the Ca^{2+} current when depletion is not suppressed by a buffering agent was then calculated as $I_{sim}^{unbuf}(t)$ from $I_{exp}^{buf}(t)$. To allow a comparison of the simulation output $I_{sim}^{unbuf}(t)$ with measurements obtained from the same fiber in unbuffered solution $I_{exp}^{unbuf}(t)$, three main assumptions were made (similar to Almers et al., 1981): 1) in Ca^{2+} buffered solution ion depletion in the TTS is completely suppressed. The currents $I_{exp}^{buf}(t)$ measured under these conditions include the L-type channel kinetics, which are assumed not to be influenced by a possible change of the extracellular Ca^{2+} concentration due to depletion of ions from the lumen of the TTS. 2) L-type Ca^{2+} channels are exclusively located in the TTS in differentiated mammalian muscle, therefore the Ca^{2+} currents only flow through the TTS membrane (see Fig. 2 *B*) and not through the surface membrane. 3) In a first approximation changes in myoplasmic free Ca^{2+} are neglected.

We used a modification of a model first proposed by Adrian et al. (1969a) and by Barry and Adrian (1973) (see Fig. 2) where the fiber is approximated by a cylinder with radial symmetry and the complete TTS is simplified as a homogenous disk with an equivalent radial conductance G_L and an equivalent voltage-dependent wall conductance $\bar{G}_W$. The TTS is connected to the extracellular space via an access resistance r_S. This disk was divided into m concentric shells and the concentration change of Ca^{2+} ions in each shell was computed numerically in discrete time intervals Δt.

Concentration changes

The concentration change in the TTS is given by the full equation of continuity (Barry and Adrian, 1973):

$$\frac{\partial c(r,t)}{\partial t} = D_{Ca}^{eff}\frac{1}{r}\frac{\partial}{\partial r}\left(r\frac{\partial c(r,t)}{\partial r}\right) - \frac{4\pi\cdot a\cdot I_{Ca}}{\rho\cdot zF}, \qquad (1)$$

where

$$I_{Ca} = -\frac{\bar{G}_W}{4\pi\cdot a}\left(V_o - V(r,t) - \frac{RT}{zF}\ln\left(\frac{c(r,t)}{c_o}\right)\right) \qquad (2)$$

denotes the calcium current flow across the tubular wall of ring n which resembles I_n^{trans} (see also Appendix). Here, c is the respective Ca^{2+} concentration (either free or total), c_o is the extracellular free Ca^{2+} concentration, R denotes the gas constant, T is the temperature in K, and F is the Faraday constant; r is the radial coordinate; t is the time; $z = 2$ is the ion valency; V_o is the potential of the sarcoplasm with respect to the external solution; $V(r, t)$ is the potential at radial distance r in the lumen of the TTS with respect to the external solution at time t; a is the fiber radius; ρ denotes the fraction of TTS volume compared to the total fiber volume.

The effective radial diffusion constant for Ca^{2+} ions in the TTS is given by Adrian et al. (1969a)

$$D_{Ca}^{eff} = \sigma D_{Ca}^{TTS}. \qquad (3)$$

The network-specific factor σ considers the contribution of the total Ca^{2+} diffusion in radial direction and is described in detail by Adrian et al. (1969a) for different types of meshes. Due to the small TTS diameter the Ca^{2+} diffusion constant in the TTS lumen, D_{Ca}^{TTS}, is slightly reduced compared to the diffusion constant D_{Ca} in free solution (Nitsche and Balgi, 1994):

$$\frac{D_{Ca}^{TTS}}{D_{Ca}} = \frac{1 + 1.125\beta\ln\beta - 1.539\beta + 1.2\beta^2}{(1-\beta)^2}, \qquad (4)$$

where

$$\beta = \frac{\text{radius}_{Ca^{2+}}}{\text{radius}_{TTS}}.$$

The time dependence of the wall conductance of the TTS, $\bar{G}_W(t)$, which forms part of I_{Ca} (see Eq. 2), is given by Barry and Adrian (1973)

$$\bar{G}_W(t) = 2\Big/\left[a\left(\frac{1}{G_T(t)} - \frac{a}{4\cdot\bar{G}_L} - r_S\right)\right], \qquad (5)$$

where $\bar{G}_L$ is the effective radial conductance (see Adrian et al. 1969a) and r_S is the access resistance as proposed by Peachey and Adrian (1973). The time-dependent total conductance of the TTS

$$G_T(t) = f_T/R_m(t) \qquad (6)$$

can be calculated from the fraction f_T of the current carried by Ca^{2+} ions compared to the total ionic current flow (Barry and Adrian, 1973). As L-type Ca^{2+} channels are almost exclusively located in the TTS (Almers et al., 1981) a typical value for f_T in our simulation was $f_T = 0.999$.

In our approach, we obtained the total time-dependent membrane resistance per unit area $R_m(t)$ by using the following relationship (Adrian et al., 1970):

$$R_m(t) = \frac{V_{clamp} - E_{Ca}}{I_{exp}^{buff}(t)}. \qquad (7)$$

In this equation, where E_{Ca} denotes the Nernst potential for calcium ions, we introduced the time dependence of the Ca^{2+} current by processing the experimentally recorded current $I_{exp}^{buff}(t)$ obtained under voltage clamp conditions with a depolarizing membrane potential V_{clamp} for a fiber bathed in Ca^{2+} buffered isotonic solution. In buffered solution, concentration changes of tubular calcium are not expected. The predominant mechanism for the decay of I_{Ca} therefore is the voltage-dependent inactivation. To correctly predict the time course of the calcium current in unbuffered solution where both the voltage dependence and the tubular Ca^{2+} depletion are present, it was necessary to consider the voltage-dependent change of $R_m(t)$ due to the concentration changes as implied by the Nernst equation.

According to Fig. 2 *B* (*right*), the Ca^{2+} concentration change in a volume element in ring n, $[dc_n(t)]/dt$, is given by the concentration decrease due to Ca^{2+} efflux from the TTS into the fiber (I_n^{trans}) and the concentration change due to Ca^{2+} diffusion from (I_{n-1}^{radial}) or into (I_n^{radial}) adjacent volume elements (see Appendix).

Voltage dependence of Ca^{2+} conductance

We used a voltage dependence for $\hat{g}(V_{clamp} - E_{Ca})$ as suggested by Dietze et al. (1998) in mouse myotubes. In essence, the current-voltage relation is described by a voltage-gated Ca^{2+} current with maximal conductance g_{max}, the driving force $V = V_{clamp} - E_{Ca}$, and experimental reversal potential V_{Ca}:

$$I(V) = \hat{g}(V) \cdot g_{max} \cdot (V - V_{Ca}) \tag{8}$$

The voltage-dependent activation of the Ca^{2+} conductance $\hat{g}$ is described by a Boltzmann function with the parameters of half-maximal activation $V_{0.5}$ and the steepness k:

$$\hat{g}(V) = 1/\{1 + \exp((V_{0.5} - V)/k)\} \tag{9}$$

Numerical simulation

The simulation was performed using an ANSI-C program running on a R10000 workstation (Silicon Graphics, IRIX 6.4). The differential equations were taken from Barry and Adrian (1973) and integrated using the fourth-order Runge-Kutta method (Ralston, 1965). The equations for the numerical computation are given in the Appendix.

Stability and convergence of the algorithm used have been tested and assured with a $\Delta t = 10^{-7}$ s for $m = 200$ shells or a $\Delta t = 3 \cdot 10^{-5}$ s for $m = 50$ shells. The resulting output data were processed using Origin 5.0 software (Microcal Software Inc., Northampton, MA).

RESULTS

As a first test of our algorithm we investigated the time course of the radial Ca^{2+} concentration $c(r, t)$ in the resting fiber when the external $[Ca^{2+}]$ is suddenly changed from zero to a new value, c_0. $c(r, t)$ is then given with the diffusion equation in cylindrical coordinates:

$$\frac{\partial c(r,t)}{\partial t} = \frac{1}{r}\frac{\partial}{\partial r}\left(rD_{Ca}^{eff}\frac{\partial c(r,t)}{\partial r}\right), \tag{10}$$

where

$$D_{Ca}^{eff} = \sigma D_{Ca}^{TTS}$$

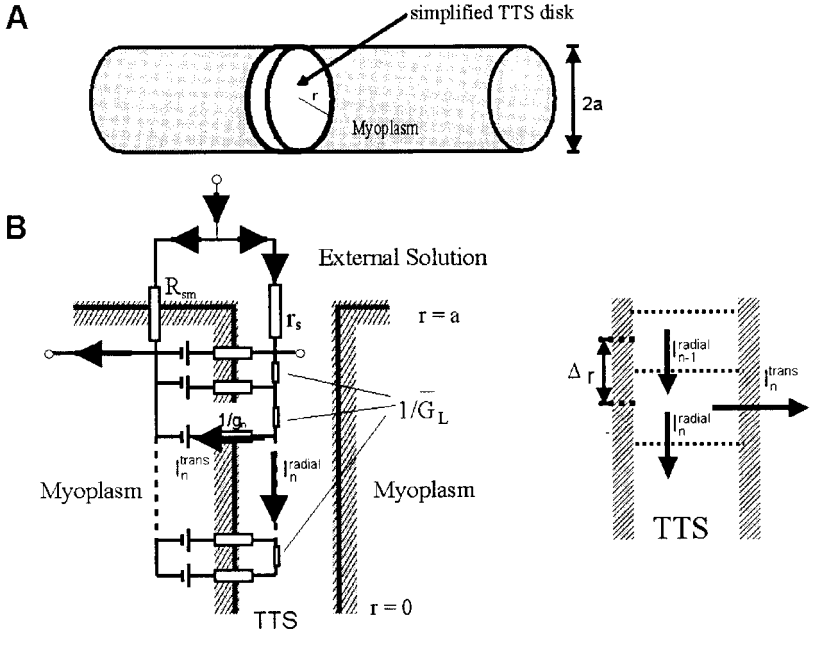

FIGURE 2 TTS geometry model used for the numerical computations. (*A*) In a simplified model with cylindrical geometry the complete TTS is reduced to a homogenous disk with equivalent conductances (modified after Barry and Adrian, 1973). (*B*) *Left*: a full schematic electrical circuit diagram of the equivalent TTS disk shown in (*A*) that is used in the numerical simulation. $1/g_n$ indicates the equivalent access resistance of ring n of the TTS (see Eq. A7 in the Appendix), $1/G_L$ is the radial resistance as described in the text. R_{sm} is the surface membrane resistance excluding the TTS. Gray arrows indicate the transverse Ca^{2+} current (I_n^{trans}) from disk n of the TTS into the fiber. (*B*) *Right*: part of the volume element at higher magnification. I_n^{trans} is the calcium current flow across the tubular wall of ring n into the fiber. I_n^{radial} is the current flow from ring n in radial direction. I_{n-1}^{radial} indicates the radial current from ring $n - 1$ into ring n of the TTS disk. Δr is the thickness of a volume element as described in the text.

with the boundary condition

$$c = c_0 \quad \text{for } r = a \quad \text{at } t > 0$$

and the initial condition

$$c = 0 \quad \text{for } 0 \le r \le a \quad \text{at } t = 0.$$

The solution of Eq. 10 for the given initial conditions is (Crank, 1975)

$$\frac{c(r,t)}{c_0} = 1 - \frac{2}{a}\sum_{n=1}^{\infty} e^{-\alpha_n^2 D_{ion}^{eff} t} \cdot \frac{J_0(r \cdot \alpha_n)}{J_1(a \cdot \alpha_n)} \qquad (11)$$

where J_0 and J_1 are Bessel functions of zero- and first-order, respectively, and the α_n are the positive roots of $J_0(a \cdot \alpha_n) = 0$.

The analytical solution of Eq. 11 was calculated with an algorithm in which the infinite sum is approximated by the first 100 terms (Uttenweiler et al., 1998) using the Maple V Rel.3 software (Waterloo Maple Inc., Ontario, Canada).

The diffusion coefficient $D_{Ca} = 7 \cdot 10^{-6}$ cm^2/s for Ca^{2+} in free solution was taken from Cannell and Allen (1984). Considering the hindered diffusional access to the TTS, Eq. 4 results in a slightly reduced diffusion coefficient $D_{Ca}^{TTS} = 6.83 \cdot 10^{-6}$ cm^2/s with radius$_{Ca^{2+}}$ = 0.106 nm (Emsley, 1989) and radius$_{TTS}$ = 25 nm. For the network considered here ($\sigma = 0.375$, Barry and Adrian, 1973) Eq. 3 leads to a resulting effective diffusion coefficient for Ca^{2+} ions in the lumen of the transverse tubular system of $D_{Ca}^{eff} = \sigma D_{Ca}^{TTS} = 2.59 \cdot 10^{-6}$ cm^2/s.

In Fig. 3, the results of the analytical concentration profiles for simple diffusion into the transverse tubular system (*circles*) are compared with the numerical output (*lines*) of the Runge-Kutta algorithm. The numerical computation deviated <0.1% from the analytical solution (see Eq. 11).

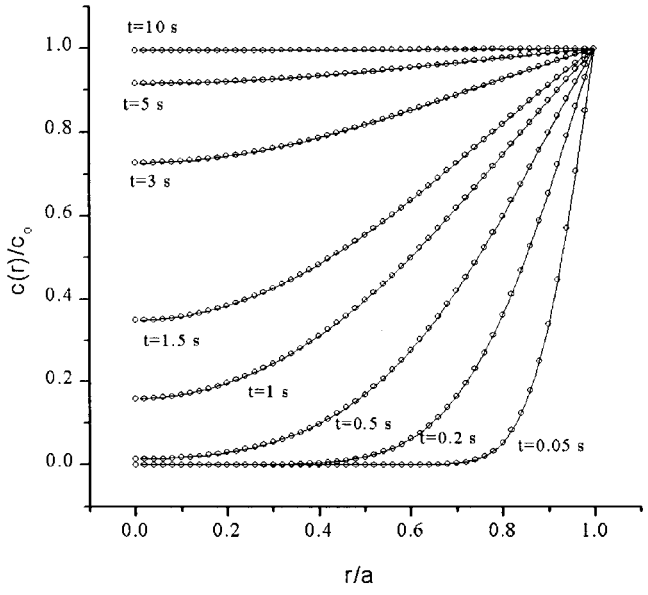

FIGURE 3 Numerical versus analytical solutions of diffusion-dependent Ca^{2+} distribution in the TTS of a murine muscle fiber. Numerical simulation (*lines*) and analytical solution (*circles*) of the Ca^{2+} distribution for inward Ca^{2+} diffusion into the TTS in the absence of any applied voltage and zero initial [Ca^{2+}] within the TTS. Fiber radius is $a = 50$ μm. Initial conditions are described in the text.

Voltage clamp data as input for the numerical simulation

As described in the Methods section, the experimentally recorded currents $I_{exp}^{buf}(t)$ obtained in isotonic buffered Ca^{2+} solution were taken as inputs for the numerical simulations. Based on $I_{exp}^{buf}(t)$ the influence of ion depletion on the time course of the currents was calculated when depletion was not suppressed by a buffering agent in the external solution. In Fig. 4, the influence of Ca^{2+} depletion on I_{Ca} recordings obtained from two representative single fibers is shown at membrane potentials of −20 mV, 0 mV, and +20 mV (Fig. 4 *A*) and at membrane potentials of −20 mV, −10 mV, 0 mV, +10 mV, +20 mV, and +30 mV (Fig. 4 *B*). Fiber dimensions were: diameter $2a = 48$ μm, length $l = 640$ μm for the fiber shown in (*A*), and $2a = 56$ μm and length $l = 592$ μm for the fiber shown in (*B*). From these fibers the recorded I_{Ca} measurements in buffered solution $I_{exp}^{buf}(t)$ (*solid red line*) and in unbuffered solution $I_{exp}^{unbuf}(t)$ (*solid black line*) are shown in each panel. $I_{exp}^{unbuf}(t)$ is then compared with the calculated numerical output $I_{sim}^{unbuf}(t)$ of the simulation model for the unbuffered trace (*blue open circles*) for a fixed parameter combination of access resistance r_s and fraction of volume ρ occupied by the TTS. For the two fibers shown the parameters $r_s = 50$ Ωcm^2, $\rho = 0.0052$ (Fig. 4 *A*) and $r_s = 125$ Ωcm^2, $\rho = 0.0053$ (Fig. 4 *B*) were kept constant for all membrane potentials during the simulation. As can be seen, for potentials up to 0 mV $I_{sim}^{unbuf}(t)$ predicted very well the time course of I_{Ca} in unbuffered solution, i.e., $I_{exp}^{unbuf}(t)$. For more positive potentials some fibers still showed good agreement between $I_{exp}^{unbuf}(t)$ and $I_{sim}^{unbuf}(t)$ as the one shown in Fig. 4 *A*, whereas in other fibers the additional outward component described in Fig. 1 became more prominent, as shown in the fiber of Fig. 4 *B*. For seven fibers tested at a temperature of 24°C the mean parameters of r_s and ρ for which the model most accurately reproduced the experimental I_{Ca} traces for a fixed parameter combination for all potentials tested were $r_s = 97.7 \pm 44.2$ Ωcm^2 and $\rho = 0.0048 \pm 0.0006$. The time constants for the decay of I_{Ca} in unbuffered solution τ_u were obtained from the output of the numerical simulation of the experimentally recorded I_{Ca} data in buffered solution. For the representative fibers shown in Fig. 4, *A* and *B* these time constants were (*A*): $\tau_u = 40$ ms at 0 mV and $\tau_u = 72$ ms at +20 mV; whereas in (*B*): $\tau_u = 167$ ms at −10 mV, $\tau_u = 80$ ms at 0 mV, $\tau_u = 98$ ms at +10 mV, $\tau_u = 113$ ms at +20 mV, and $\tau_u = 129$ ms at +30 mV. The I_{Ca} decay time constants for the experimental traces in buffered solution were $\tau_b = 254$

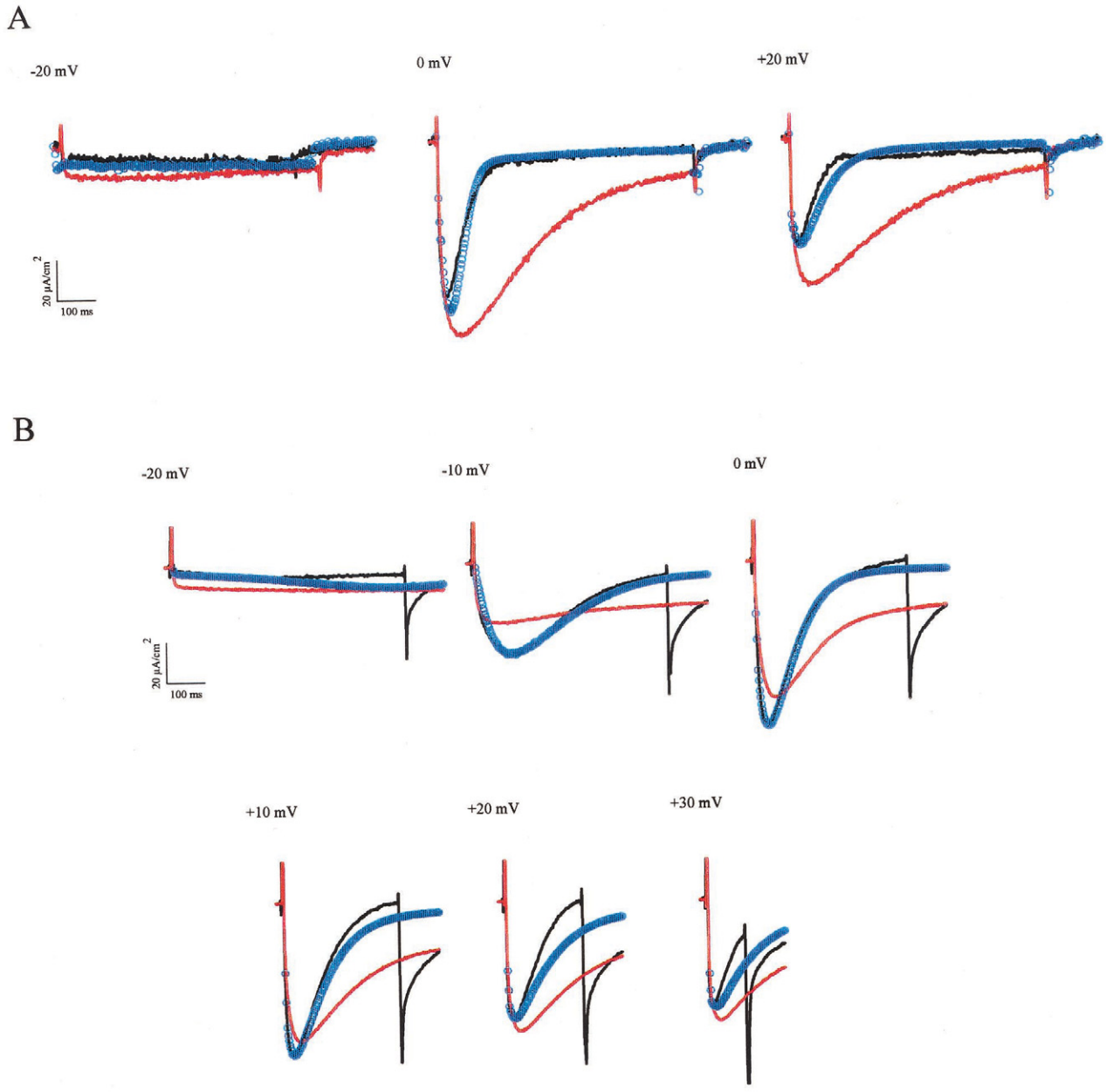

FIGURE 4 The experimental time course of the decay of I_{Ca} in unbuffered solution is well-predicted by the results of the model. Time courses of the experimentally recorded I_{Ca} in buffered isotonic solution $I_{exp}^{buf}(t)$ (*solid red line*) and in unbuffered solution $I_{exp}^{unbuf}(t)$ (*solid black line*) versus simulation for two representative fibers bathed in isotonic solution at 30°C for three potentials (−20 mV, 0 mV, and +20 mV, *A*) and at 24°C for six membrane potentials (−20 mV, −10 mV, 0 mV, +10 mV, +20 mV, and +30 mV, *B*). Fiber dimensions were: radius $a = 28$ μm, length $l = 592$ μm (*A*) and $a = 24$ μm, $l = 640$ μm (*B*). A constant parameter combination for the access resistance r_s and the fraction of volume occupied by the TTS ρ was used for all potentials in the simulation: (*A*) $r_s = 50$ Ωcm^2, $\rho = 0.0052$, and $r_s = 125$ Ωcm^2, $\rho = 0.0053$ (*B*). $I_{exp}^{buf}(t)$ was used as input data for the numerical simulation and the simulated time course of I_{Ca} in unbuffered solution $I_{sim}^{unbuf}(t)$ is shown (*blue circles*) for each membrane potential. Note that the experimental time course of $I_{exp}^{unbuf}(t)$ is well-reproduced by the numerical simulation for membrane potentials up to +20 mV in (*A*) and up to 0 mV in (*B*). In some fibers (e.g., *B*) the experimental I_{Ca} in unbuffered solution declines faster for higher depolarizations (e.g., more positive than 0 mV, *B*) than predicted by the model presumably due to an additional outward component as shown in Fig. 1.

ms at 0 mV, $\tau_b = 312$ ms at +20 mV (*A*), and $\tau_b = 255$ ms at −10 mV, $\tau_b = 118$ ms at 0 mV, $\tau_b = 184$ ms at +10 mV, $\tau_b = 235$ ms at +20 mV, and $\tau_b = 184$ ms at +30 mV (*B*). In Fig. 5 the averaged I_{Ca} decay time constants for different fibers bathed in isotonic calcium unbuffered (τ_u, *solid bars*) and calcium buffered solution (τ_b, *dashed bars*) at three different membrane potentials (−10 mV, 0 mV, and +10 mV) are shown. The mean time constants in the buffered solution (τ_b) were 230 ± 75 ms at −10 mV ($n = 4$), 144 ± 39 ms at 0 mV ($n = 7$), and 144 ± 31 ms at +10 mV ($n =$

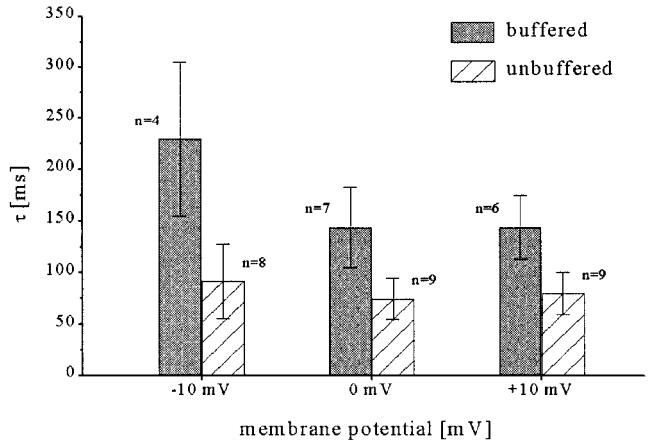

FIGURE 5 I_{Ca} decay time constants for single fibers bathed in calcium-buffered (τ_b) and unbuffered (τ_u) solution obtained from the numerical simulation. Comparison of the decay time constants at membrane potentials of −10 mV, 0 mV, and +10 mV in unbuffered (τ_u, *dashed bars*) and buffered (τ_b, *solid bars*) solution. Data are given as mean ± SD. The time constants had significant smaller values in unbuffered solution compared to buffered solution for all potentials tested ($p < 0.0012$). On average, the ratios τ_b/τ_u were 2.51 at −10 mV, 1.92 at 0 mV, and 1.79 at +10 mV.

6). The τ_b values were significantly larger than the time constants in unbuffered solution τ_u ($p < 0.013$ for all potentials tested, Student's unpaired *t*-test) which were 92 ± 36 ms at −10 mV ($n = 8$), 75 ± 20 ms at 0 mV ($n = 9$), and 80 ± 20 ms at +10 ms ($n = 9$). On average, the ratios τ_b/τ_u were 2.51 at −10 mV, 1.92 at 0 mV, and 1.79 at +10 mV.

Resulting calcium concentration in the TTS

As an example for the size of the tubular Ca^{2+} depletion the time course of the radial calcium concentration $[Ca^{2+}](r, t)$ for the fiber shown in Fig. 4 *A* is shown in Fig. 6. The left plot shows the time- and spatial-dependent $[Ca^{2+}](r, t)$ for a membrane potential of 0 mV, the right plot for a membrane potential of +20 mV. The steady-state averaged $[Ca^{2+}]$ values for this fiber were 7.5 mM at −20 mV (not shown), 1.05 mM at 0 mV, and 2.56 mM at +20 mV; whereas the calculated steady-state $[Ca^{2+}]$ values in the fiber center were 6.5 mM at −20 mV (not shown), 0.7 mM at 0 mV, and 1.53 mM at +20 mV. Note that the calcium concentration in the fiber center ($r/a = 0$) drops to a value of <7% of its initial value.

DISCUSSION

The aim of this work was to study whether the faster decline of slowly activating L-type calcium currents I_{Ca} in single mammalian muscle fibers under maintained depolarization might be explained by the substantial change in ion concentration in the small lumen of the tubular system. In skeletal muscle fibers the decline of Ca^{2+} currents in physiologically isotonic unbuffered Ca^{2+} solution is up to three times faster than currents recorded from the same fiber in Ca^{2+} buffered solution, where no Ca^{2+} depletion should occur (Friedrich et al., 1999).

It should be noted that despite the very detailed and elegant investigations of the electrical properties of the TTS (Gage and Eisenberg, 1969; Eisenberg and Gage, 1969;

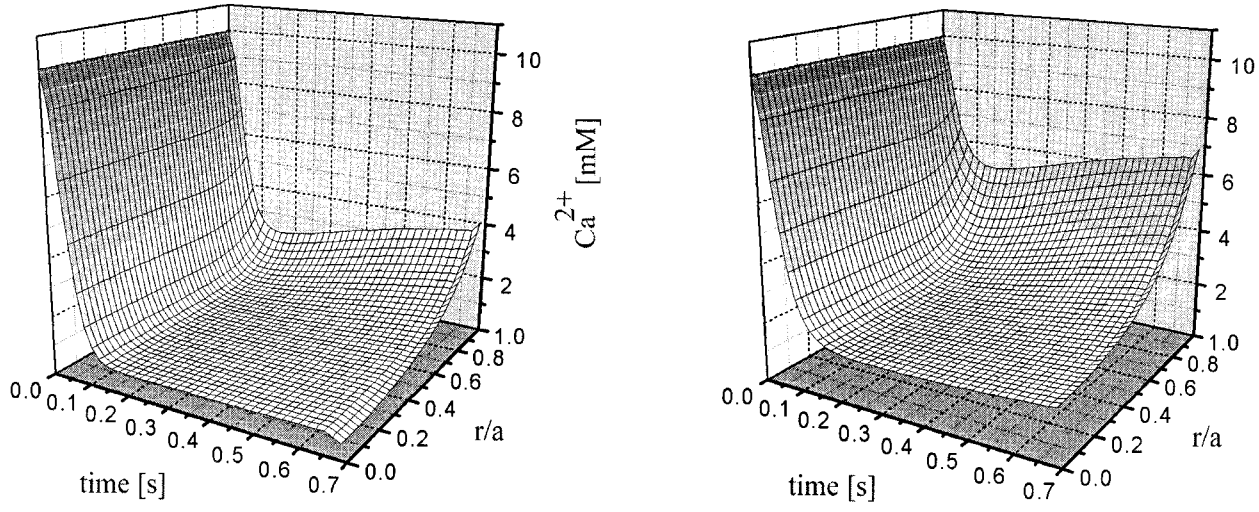

FIGURE 6 Radial and time-dependent calcium concentration profiles in a single fiber at different membrane potentials. The resulting radial and time-dependent calcium concentration $[Ca^{2+}](r, t)$ in the transverse tubular system for the representative single fiber shown in Fig. 4 *A* at a membrane potential of 0 mV (*left plot*) and +20 mV (*right plot*). Note that the calcium concentration in the fiber center ($r/a = 0$) drops to a value of ~7% of its initial value. The steady-state averaged $[Ca^{2+}]$ values for this fiber were 1.05 mM at 0 mV and 2.56 mM at +20 mV, whereas the calculated steady-state $[Ca^{2+}]$ values in the fiber center were 0.7 mM at 0 mV and 1.53 mM at +20 mV.

Valdiosera et al., 1974a, 1974b; Eisenberg et al., 1977; Mathias et al., 1977; Levis et al., 1983) there is still a lack of quantitative knowledge about the time- and space-dependent ion concentration changes caused by membrane currents. There are also very detailed structural investigations of the TTS (for review see, e.g., Peachey and Franzini-Armstrong, 1983) and different models for its mathematical treatment (for review see, e.g., Eisenberg, 1983). However, as we focused on the ionic current and the concentration changes, we decided to carry out simulations based on the early work of Adrian et al. (1969a, 1969b).

The analysis was simplified by the fact that the Ca^{2+} current flows almost exclusively across the TTS membrane. Therefore it is possible to use the Ca^{2+} current measurement in Ca^{2+} buffered solution as an input for the calculation of the time course of depletion development in the TTS.

To introduce the voltage dependence of I_{Ca} activation, we basically used data by Dietze et al. (1998), as they have been obtained in skeletal myotubes, though our data can also be fitted by the voltage dependence introduced by Jafri et al. (1998) for cardiac tissue.

Aside from the fixed parameters listed in Table 1 we had to adjust only the values of ρ and r_s to accurately fit our experimental data under experimental conditions where the outward component could be neglected. For the fractional lumen of the TTS we found a mean value of $\rho = 0.0048 \pm 0.0006$, which agrees well with that of between 0.005 and 0.006 determined in mammalian laryngeal and sternomastoid muscle fibers by Hinrichsen and Dulhunty (1982). Besides the lumen of the TTS, we found the access resistance r_s to be the essential parameter for adjusting the steady-state value of the simulation output $I_{sim}^{unbuf}(t)$ to the experimentally recorded current $I_{exp}^{unbuf}(t)$. The best fit for fibers in isotonic solution was obtained with values ranging from $r_s = 35\ \Omega cm^2$ to $r_s = 175\ \Omega cm^2$. Our range with a mean value of $r_s = 97.7 \pm 44.2\ \Omega cm^2$ is in good agreement with that found in other studies. A value of $r_s = 150\ \Omega cm^2$ was proposed by Adrian and Peachey (1973). In a previous study on the potential distribution in the TTS after application of supercharging pulses, Kim and Vergara (1998) reported values in the range of 110–150 Ωcm^2 for frog skeletal muscle. From impedance measurements of frog skeletal muscle, Valdiosera et al. (1974b) found access resistance values in the range of 120–130 Ωcm^2. The lower part of our range is consistent with values of 20–50 Ωcm^2 reported by Heiny et al. (1983) obtained from a fit to absorbance of a potentiometric dye transient. For rat skeletal muscle Simon and Beam (1985) report a value of $r_s = 60\ \Omega cm^2$ obtained from a fit to charge movements.

With our approach, we are able to directly calculate and quantify the influence of ion depletion on the time course of the slowly activating calcium current for a skeletal muscle fiber. For a representative fiber with a diameter of 48 μm and a fiber length of 640 μm, we found that the Ca^{2+} concentration in the fiber center can drop to a value of only 7% of the initial value. In some fibers with a larger diameter we observed a reduction to a minimal value of 3% of the initial Ca^{2+} concentration (not shown). Such pronounced Ca^{2+} depletion is also likely to occur in other cells with diffusion-restricted spaces, e.g., in sheep Purkinje strands (Levis et al., 1983) and in neural tissue (Egelman and Montague, 1999). Furthermore, our simulated data in unbuffered solution I_{sim}^{unbuff} is in very good agreement with the experimental data I_{exp}^{unbuff} without the need of introducing a Ca^{2+}-induced I_{Ca} inactivation as proposed by Neely et al. (1994) for the cardiac Ca^{2+} channel alpha 1 subunit (alpha 1C) expressed in *Xenopus* oocytes.

In the present study we confirm the hypothesis that Ca^{2+} depletion in the transverse tubular system of single skeletal muscle fibers significantly influences the time course of ionic currents. Interestingly, our results are in agreement with previous findings on the time course of I_{Ca} in cardiac sheep Purkinje strands (Levis et al., 1983) where the depletion of calcium was enough to explain the turn-off of calcium current without invoking the inactivation process.

Furthermore, Blatter and Niggli (1998) used laser-scanning confocal microscopy to detect extracellular [Ca^{2+}] and changes of t-tubular [Ca^{2+}] in cardiac myocytes. The authors reported a slow exchange of solution in the t-tubular system, suggesting a depletion of Ca^{2+} ions in the TTS of cardiac myocytes during physiological activity. Thus, it would be most interesting to test this suggestion by follow-

TABLE 1 Parameters used for simulations

Definition	Symbol and Value	Reference
Free Ca^{2+} diffusion constant	$D_{Ca}^{free} = 7 \times 10^{-6}$ cm^2/s	Cannell and Allen, 1984
Ca^{2+} diffusion constant in tubular lumen	$D_{Ca}^{TTS} = 6.9 \times 10^{-6}$ cm^2/s	Nitsche and Balgi, 1994
Effective radial diffusion coefficient in the TTS	$D_{Ca}^{eff} = 2.59 \times 10^{-6}$ cm^2/s	
Extracellular [Ca^{2+}]	$C_o = 10$ mM	
Intracellular [Ca^{2+}]	$C_i = 100$ nM	
Ca^{2+} equilibrium potential (23°C)	$E_{Ca} = +144$ mV	Nernst equation
Network factor	$\sigma = 0.375$	Adrian et al., 1969a
Conductance of tubular lumen	$G_L = 0.01$ S/cm	Barry and Adrian, 1973
Fraction of Ca^{2+} conductance in the TTS of total conductance	$f_T = 0.999$	
Number of rings	$m = 200$	
Size of time step	$\Delta t = 2.5 \times 10^{-8}$ s	

ing the changes in tubular Ca^{2+} concentration in mammalian muscle with fluorescence indicators and apply our combined experimental and simulation approach.

APPENDIX

The aim of this appendix is to show our extension of the model developed by Barry and Adrian (1973). The simulations were based on the original source code, developed by P. H. Barry for his simulation of potassium depletion in the TTS of skeletal muscle fibers during hyperpolarizing pulses. Here we present the equations used in the numerical model, all of which are taken from Barry and Adrian (1973). The basic approach for the model was given by:

$$\frac{dc_n}{dt} = f(t, c_n) \tag{A1}$$

$$c_n(t + \Delta t) = c_n(t) + \frac{(K1_n + 2K2_n + 2K3_n + K4_n)}{6}, \tag{A2}$$

where c_n denominates the respective Ca^{2+} concentration in the nth ring, t is the time, Ki_n are the Runge-Kutta coefficients specified below, and $f(t, c_n)$ is given by the difference between the loss of Ca^{2+} due to the transport number effect (caused by the current through the TTS wall) and the increase due to radial diffusion, as shown in Eqs. 1 and 2.

$$f(t, c_n) = a1_n \cdot (c_{n-1}(t) - c_n(t)) - a2_n \cdot (c_n(t) - c_{n+1}(t)) - a3_n \cdot I_n^{trans}(t) \tag{A3}$$

where

$$a1_n = D_{Ca}^{eff}(m - n + 1)/((\Delta r)^2 \cdot (m - n + 0.5))$$
$$a2_n = D_{Ca}^{eff}(m - n)/((\Delta r)^2 \cdot (m - n + 0.5))$$
$$a3_n = a/(\rho \cdot F \cdot (\Delta r)^2 \cdot (m - n + 0.5)),$$

with D_{Ca}^{eff} as the effective radial diffusion coefficient in the TTS (see Table 1), a the fiber radius, n the actual and m the total number of concentric shells of the TTS disk, F the Faraday constant, ρ the fraction of the fiber volume occupied by the TTS, r the radius of the concentric shell, and Δr the thickness of a single ring given by $\Delta r = a/m$.

At the fiber surface ($n = 1$) A3 is given by

$$f(t, c_1) = a1_n \cdot (c_0(t) - [c_1(t) + 0.5 \cdot \{c_1(t) - c_2(t)\}]) - a2_1 \cdot (c_1(t) - c_2(t)) - a3_1 \cdot I_1^{trans}(t) \tag{A3a}$$

where

$$a1_1 = (m \cdot D_{Ca}^{eff})/(\Delta r \cdot r_S \cdot \bar{G}_L \cdot (m - 0.5)),$$

with the access resistance r_s of the tubular lumen and $\bar{G}_L$ the effective radial conductance (Adrian et al., 1969a).

The Runge-Kutta coefficients are

$$K1_n = \Delta t \cdot f(t, c_n) \tag{A4a}$$

$$K2_n = \Delta t \cdot f\left(t + \frac{\Delta t}{2}, c_n + \frac{K1_n}{2}\right) \tag{A4b}$$

$$K3_n = \Delta t \cdot f\left(t + \frac{\Delta t}{2}, c_n + \frac{K2_n}{2}\right) \tag{A4c}$$

$$K4_n = \Delta t \cdot f(t + \Delta t, c_n + K3_n). \tag{A4d}$$

The current I_n^{trans} of ring n passing through the TTS wall into the fiber is given by:

$$I_n^{trans}(t) = G_n(t) \cdot \frac{(m - n + 0.5)}{a} \Delta r^2 \cdot V_n^{rel}(t) \tag{A5}$$

where

$$V_n^{rel}(t) \equiv V(t) - E_{Ca} = V_o - V_n(t) - \frac{RT}{2 \cdot F} \ln\left(\frac{c_n(t)}{c_0}\right) \tag{A6}$$

is the driving force for the ionic current and

$$G_n(t) = \bar{G}_W(t) \cdot \hat{g}(V) \cdot (\Delta r)^2 (m - n + 0.5)/a \tag{A7}$$

is the conductance of ring n. $\bar{G}_W$ is the voltage-dependent wall conductance of the TTS, $\hat{g}(V)$ is the apparent driving force for I_{Ca}, and V_o is the membrane potential during the voltage clamp pulse. V_n is the potential difference at the center of ring n with respect to the external solution and is given by

$$V_{n+1}(t) = V_n(t) - \frac{I_n^{radial}(t) \cdot a \cdot \ln\left\{\frac{m - n + 0.5}{m - n - 0.5}\right\}}{G_L}, \tag{A8}$$

where G_L is an equivalent radial conductance of the simplified homogenous disk of the TTS. $I_n^{radial}(t)$ represents the radial current leaving ring n toward the fiber center and is given by:

$$I_n^{radial}(t) = I_{n-1}^{radial}(t) - I_n^{trans}(t) \tag{A9}$$

The termination criteria for the calculation of $\Delta I = I_{m-1}^{radial} - I_m^{trans}$ was set to $\Delta I < 10^{-20}$.

This work was supported by a grant from the German Research Foundation Deutsche Forschungsgemeinschaft (DFG, Graduiertenkolleg 388, "Biotechnologie") and DFG research unit Image Sequence Analysis to Investigate Dynamic Processes, FOR 240/2-2. This work is part of a Ph.D. thesis of T. Ehmer.

REFERENCES

Adrian, R. H., W. K. Chandler, and A. L. Hodgkin. 1969a. The kinetics of mechanical activation in frog muscle. *J. Physiol.* 204:207–230.

Adrian, R. H., W. K. Chandler, and A. L. Hodgkin. 1970. Voltage clamp experiments in striated muscle fibres. *J. Physiol.* 208:607.

Adrian, R. H., L. L. Costantin, and L. D. Peachey. 1969b. Radial spread of contraction in frog muscle fibres. *J. Physiol.* 204:231–257.

Adrian, R. H., and L. D. Peachey. 1973. Reconstruction of the action potential of frog sartorius muscle. *J. Physiol.* 235:103–131.

Almers, W., R. Fink, and P. T. Palade. 1981. Calcium depletion in frog muscle tubules: the decline of calcium current under maintained depolarisation. *J. Physiol.* 312:177–207.

Almers, W., and P. T. Palade. 1981. Slow calcium and potassium currents across frog muscle membrane: measurements with a vaseline-gap technique. *J. Physiol.* 312:159–176.

Amsellem, J., R. Delorme, C. Souchier, and C. Ojeda. 1995. Transverse-axial tubular system in guinea pig ventricular cardiomyocyte: 3D reconstruction, quantification and its possible role in K^+ accumulation-depletion phenomenon in single cells. *Biologie Cellulaire* 85:43–54.

Barry, P. H., and R. H. Adrian. 1973. Slow conductance changes due to potassium depletion in the transverse tubules of frog muscle fibers during hyperpolarizing pulses. *J. Membr. Biol.* 14:243–292.

Beaty, G. N., and E. Stefani. 1976. Inward calcium current in twitch muscle fibres of the frog. *J. Physiol.* 260:27P.

Blatter, L. A., and E. Niggli. 1998. Confocal near membrane detection of calcium in cardiac myocytes. *Cell Calcium.* 23:269–279.

Cannell, M. B., and D. G. Allen. 1984. Model of calcium movement during activation in the sarcomere of frog skeletal muscle. *Biophys. J.* 45: 913–925.

Cota, G., L. Nicola-Siri, and E. Stefani. 1983. Calcium-channel gating in frog skeletal muscle membrane: effects of temperature. *J. Physiol.* 338:395–412.

Cota, G., L. Nicola-Siri, and E. Stefani. 1984. Calcium channel inactivation in frog (*Rana pipiens* and *Rana montezuma*) skeletal muscle fibres. *J. Physiol.* 354:99–108.

Cota, G., and E. Stefani. 1989. Voltage-dependent inactivation of slow calcium channels in intact twitch muscle fibers of the frog. *J. Gen. Physiol.* 94:937–951.

Crank, J. 1975. The Mathematics of Diffusion. Oxford University Press.

Dietze, B., F. Bertocchini, V. Barone, A. Struck, V. Sorrentino, and W. Meltzer. 1998. Voltage-controlled Ca^{2+} release in normal and ryanodine receptor type 3 (RyR3)-deficient mouse myotubes. *J. Physiol.* 513.1: 3–9.

Dulhunty, A. 1982. Effect of chloride withdrawal on the geometry of the T-tubules in amphibian and mammalian muscle. *J. Membr. Biol.* 67: 81–90.

Egelman, D. M., and P. R. Montague. 1999. Calcium dynamics in the extracellular space of mammalian neural tissue. *Biophys. J.* 76: 1856–1867.

Eisenberg, R. S. 1983. Impedance measurement of the electrical structure of skeletal muscle. *In* Handbook of Physiology, Section 10: Skeletal Muscle, Chapter 2. L. D. Peachey, R. H. Adrian, and S. R. Geiger, editors. American Physiological Society, Bethesda, MD. 301–324.

Eisenberg, R. S., and P. W. Gage. 1969. Ionic conductances of the surface and transverse tubular membranes of frog sartorius fibers. *J. Gen. Physiol.* 53:279–297.

Eisenberg, R. S., R. T. Mathias, and J. S. Rae. 1977. Measurement, modeling, and analysis of the linear electrical properties of cells. *Ann. NY. Acad. Sci.* 303:342–354.

Emsley, J. 1989. The Elements. Clarendon Press, London.

Francini, F., L. Pizza, and G. Traina. 1992. Inactivation of the slow calcium currents in twitch skeletal muscle fibres of the frog. *J. Physiol.* 448: 633–653.

Francini, F., and E. Stefani. 1989. Decay of the slow calcium current in twitch muscle fibers of the frog is influenced by intracellular EGTA. *J. Gen. Physiol.* 94:953–969.

Friedrich, O., T. Ehmer, and R. H. A. Fink. 1999. Calcium currents during contraction and shortening in enzymatically isolated murine skeletal muscle fibres. *J. Physiol.* 517.3:757–770.

Gage, P., and R. S. Eisenberg. 1969. Capacitance of the surface and transverse tubular membrane of frog sartorius muscle fibers. *J. Gen. Physiol.* 53:265–278.

García, J., K. McKinley, S. H. Appel, and E. Stefani. 1992. Ca^{2+} current and charge movement in adult single human skeletal muscle fibres. *J. Physiol.* 454:183–196.

Heiny, J. A., F. M. Ashcroft, and J. M. Vergara. 1983. T-system optical signals associated with inward rectification in skeletal muscle. *Nature.* 301:164–166.

Hinrichsen, C., and A. Dulhunty. 1982. The contractile properties, histochemistry, ultrastructure and electrophysiology of the cricothyroid and posterior cricoarytenoid muscles in the rat. *J. Muscle Res. Cell Motil.* 3:169–190.

Jafri, M. S., J. J. Rice, and R. L. Winslow. 1998. Cardiac Ca^{2+} dynamics: the roles of ryanodine receptor adaption and sarcoplasmic reticulum load. *Biophys. J.* 74:1149–1169.

Kim, A. M., and J. L. Vergara. 1998. Supercharging accelerates T-tubule membrane potential changes in voltage clamped frog skeletal muscle fibers. *Biophys. J.* 75:2098–2116.

Lamb, G. D., and T. Walsh. 1987. Calcium currents, charge movement and dihydropyridine binding in fast- and slow-twitch muscles of rat and rabbit. *J. Physiol.* 393:595–617.

Levis, R. A., R. T. Mathias, and R. S. Eisenberg. 1983. Electrical properties of sheep Purkinje strands. Electrical and chemical potentials in the clefts. *Biophys. J.* 44:225–248.

Lorkovic, H., and R. Rüdel. 1983. Influence of divalent cations on potassium contracture duration in frog muscle fibres. *Pflügers Arch.* 398: 114–119.

Mathias, R. T., R. S. Eisenberg, and R. Valdiosera. 1977. Electrical properties of frog skeletal muscle fibers interpreted with a mesh model of the tubular system. *Biophys. J.* 17:57–93.

Miledi, R., I. Parker, and P. H. Zhu. 1983. Changes in threshold for calcium transients in frog skeletal muscle fibres owing to calcium depletion in the T-tubules. *J. Physiol.* 344:233–241.

Neely, A., R. Olcese, X. Wei, L. Birnbaumer, and E. Stefani. 1994. Ca^{2+}-dependent inactivation of a cloned cardiac Ca^{2+} channel alpha 1 subunit (alpha 1C) expressed in *Xenopus* oocytes. *Biophys. J.* 66: 1895–1903.

Nicola-Siri, L., J. A. Sanchez, and E. Stefani. 1980. Effect of glycerol treatment on the calcium current of frog skeletal muscle. *J. Physiol.* 305:87–96.

Nitsche, J. M., and G. Balgi. 1994. Hindered Brownian diffusion of spherical solutes within circular cylindrical pores. *Industrial and Engineering Chemistry Research.* 33:2242–2247.

Peachey, L. D. 1965. The sarcoplasmic reticulum and transverse tubules of the frog's sartorius. *J. Cell Biol.* 25:209–231.

Peachey, L. D., and R. H. Adrian. 1973. Electrical properties of the transverse tubular system. *In* Structure and Function of muscle, Vol. III. Physiology and Biochemistry. 2nd Ed. G. H. Bourne, editor. Academic Press, Inc., New York.

Peachey, L. D., and C. Franzini-Armstrong. 1983. Structure and function of membrane systems of skeletal muscle. *In* Handbook of Physiology, Section 10: Skeletal Muscle, Chapter 2. L. D. Peachey, R. H. Adrian and S. R. Geiger, editors. American Physiological Society, Bethesda, MD. 23–71.

Ralston, A. 1965. A First Course in Numerical Analysis. McGraw Hill Book Co., Inc., New York.

Sánchez, J. A., and E. Stefani. 1978. Inward calcium current in twitch muscle fibres of the frog. *J. Physiol.* 283:197–209.

Sánchez, J. A., and E. Stefani. 1983. Kinetic properties of calcium channels of twitch muscle fibres of the frog. *J. Physiol.* 337:1–17.

Simon, B. J., and K. G. Beam. 1985. The influence of transverse tubular delays on the kinetics of charge movement in mammalian skeletal muscle. *J. Gen. Physiol.* 85:21–42.

Stanfield, P. R. 1977. A calcium dependent inward current in frog skeletal muscle fibres. *Pflügers Arch.* 368:267–270.

Uttenweiler, D., and R. H. A. Fink. 1999. Mathematical modeling of Ca^{2+}-transients measured with fluorescence imaging. *In* Handbook of Computer Vision and Applications. B. Jähne, H. Haussecker, and P. Geissler, editors. Academic Press, New York. 737–750.

Uttenweiler, D., C. Weber, and R. H. A. Fink. 1998. Mathematical modeling and fluorescence imaging to study the Ca^{2+} turnover in skinned muscle fibers. *Biophys. J.* 74:1640–1653.

Valdiosera, R., C. Clausen, and R. S. Eisenberg. 1974a. Circuit models of the passive electrical properties of frog skeletal muscle fibers. *J. Gen. Physiol.* 63:432–459.

Valdiosera, R., C. Clausen, and R. S. Eisenberg. 1974b. Impedance of frog skeletal muscle fibers in various solutions. *J. Gen. Physiol.* 63:460–491.